Available online at www.sciencedirect.com
ScienceDirect
Scripta Materialia 64 (2011) 390–393
Scripta MATERIALIA
www.elsevier.com/locate/scriptamat

# On the formation of vacancies in α-ferrite of a heavily cold-drawn pearlitic steel wire

Y.Z. Chen,[a,*] G. Csiszár,[b] J. Cizek,[c] C. Borchers,[a] T. Ungár,[b] S. Goto[d] and R. Kirchheim[a]

[a]*Institut für Materialphysik, Universität Göttingen, 37077 Göttingen, Germany*
[b]*Department of Materials Physics, Eötvös University, Budapest H-1518 POB, Hungary*
[c]*Department of Low-Temperature Physics, Charles University in Prague, V Holesovickach 2 CZ-18000 Praha 8, Czech Republic*
[d]*Department of Materials Science and Engineering, Akita University, Akita 010-8502, Japan*

Received 9 August 2010; revised 23 October 2010; accepted 27 October 2010
Available online 3 November 2010

Cold-drawn pearlitic steel wires are widely used in numerous engineering fields. Combining X-ray line profile analysis and positron annihilation spectroscopy methods, up to $10^{-5}$–$10^{-4}$ vacancies were found in α-ferrite of a cold-drawn pearlitic steel wire with a true strain of $\varepsilon = 3$. The formation of deformation-induced vacancies in α-ferrite of cold-drawn pearlitic steel wire was quantitatively testified.


*Keywords:* Pearlitic steel; Severe plastic deformation; Vacancies; X-ray diffraction; Positron annihilation

Cold-drawn pearlitic steel wires have a great potential of applications in industrial fields. Pearlitic steel consists of α-ferrite and cementite [1]. After cold drawing, cementite partially dissolves, while α-ferrite is severely deformed [1–3] and a high density of defects, e.g. dislocations and vacancies, is produced. The role of dislocations, has attracted much attention [2,4–7]. Less attention has been paid to the role of vacancies, besides being discussed in a recent study on recovery and thermal stability of heavily cold-drawn pearlitic steel wires [8]. Vacancy agglomeration is expected to be a potential source of fracture initiation [9], which could be an important factor influencing the performance of these widely used materials. However, the corresponding research in cold-drawn pearlitic steel wire is still scarce, due to a lack of direct evidence for the existence of deformation-induced vacancies.

Positron annihilation spectroscopy (PAS) has proved to be the most powerful method for the detection of point defects [10]. Saturated positron trapping often occurs in severely deformed metals containing a very high density of defects, and prevents direct determination of defect densities by application of the simple trapping model [11]. In this case, one can only determine the ratio of positron trapping rates of vacancies and dislocations. In order to estimate the concentration of vacancies, the dislocation density should be quantitatively determined by some independent technique. By evaluating the Bragg peak broadening of X-ray diffraction (XRD) patterns, X-ray line profile analysis (XLPA) can be used to evaluate dislocation densities [12–14]. The combination of XLPA and some other vacancy sensitive methods has been applied to study the deformation-induced point defects in plastically deformed copper (cf. Ref. [15]). In this letter, the vacancy concentration in a cold-drawn pearlitic steel wire with a true strain of $\varepsilon = 2\ln(d_i/d_f) = 3$ with $d_i$ (=1.669 mm) the diameter of the initial wire and $d_f$ (=0.3695 mm) the diameter of the as-drawn wire was estimated by combining PAS and XLPA. We provide direct evidence for the deformation-induced vacancies in cold-drawn pearlitic steel wire.

The wire specimens used in the present study were provided by Nippon Steel Corporation. The initial wire with a composition of Fe–0.82C–0.20Si–0.50Mn–0.005P–0.004S (wt.%) was first austenitized at 1223 K and then patented in a lead bath at 833 K for 20 s. This as-patented wire was then drawn to a true strain of 3 by a wet drawing method. The detailed procedure is described elsewhere [16]. During the cold drawing, the temperature of wires did not exceed 373 K. Annealing treatment was performed in a high vacuum furnace and subsequently cooled down to room temperature in the furnace. XRD measurements were carried out with Co $K\alpha$ radiation

* Corresponding author. E-mail addresses: yuzeng@ump.gwdg.de; chyzeng_nwpu@163.com

1359-6462/$ - see front matter © 2010 Acta Materialia Inc. Published by Elsevier Ltd. All rights reserved.
doi:10.1016/j.scriptamat.2010.10.039

following the procedures described in Ref. [17]. Positron lifetime measurements were performed using a digital PAS spectrometer with a time resolution of 145 ps (full width at half maximum, $^{22}$Na) [18]. Positron lifetime spectra, which contain at least $10^7$ positron annihilation events, were decomposed into exponential components using a maximum likelihood based fitting procedure [19]. PAS specimens were prepared by packing the wires into high-purity paraffin. The dimensions of each PAS specimen were $(10 \times 10 \times 1)$ mm$^3$. After packing, the sample surface was cleaned with heptane to partially remove the paraffin covering the top of the steel wires. Hence, bare steel wires are exposed to the irradiation source. The positron source encapsulated by mylar thin foils (2 μm)was sandwiched between two identical samples, see Figure 1. Using a bare paraffin reference specimen, it was determined that no contribution corresponding to positrons annihilated in paraffin was detected in the PAS spectra. This verified that packed steel wire samples are appropriate for PAS measurements.

X-ray line profiles obtained by integrating the whole Debye–Scherrer rings are shown in Figure 2. The peaks corresponding to cementite are rather weak. In the as-patented wire, those peaks are only visible around the (1 1 0) peak of α-ferrite, while in the as-drawn wire, due to the partial dissolution and/or pronounced peak broadening of cementite, the cementite peaks are not detectable. The α-ferrite Bragg peaks show significant broadening after cold drawing. The broadening of Bragg peaks can be caused by size broadening and strain broadening [20–23]. Applying XLPA to the measured XRD patterns, the contributions of size broadening and strain broadening to the Bragg peaks of α-ferrite were studied. The analyses were performed following the extended convolutional multiple whole-profile (eCMWP) procedures [22–24]. The physical parameters used in eCMWP fitting are Burgers vector $b = 0.248$ nm [10], average dislocation contrast factor $C_{h00} = 0.256$ [12,25] and lattice parameter $a = 0.2866$ nm. Figure 3 presents an example of the eCMWP fitting. The dislocation densities $\rho_D$(as-patented) $= (8 \pm 2) \times 10^{14}$ m$^{-2}$ and $\rho_D$(as-drawn) $= (8 \pm 1) \times 10^{15}$ m$^{-2}$ were determined.

Positron trapping in the pearlitic steel wire may occur inside cementite or α-ferrite. However, since positron affinity in cementite is much higher than in α-ferrite [26], the positron ground state energy in α-ferrite is lower than in cementite. As the observed width of cementite lamellae, 3–7 nm [1], is more than one order of magnitude smaller than the mean positron diffusion length in transition metals, 100–150 nm [26–28], positrons stopped inside cementite lamellae diffuse into α-ferrite regions.

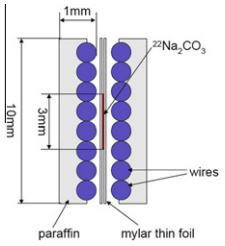


**Figure 1.** Schematic illustration of the sample arrangement during the PAS measurement.

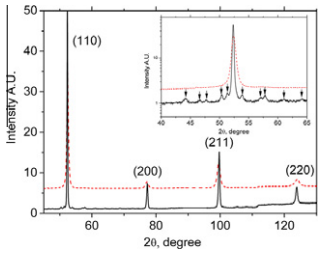


**Figure 2.** Typical measured diffraction patterns with a linear intensity scale of the as-patented wire (solid line) and the as-drawn wire (dashed line). The inset is the enlarged part of the patterns around the (1 1 0) reflection of the α-ferrite phase with a logarithmic intensity scale revealing the peaks corresponding to cementite (indicated by arrows).

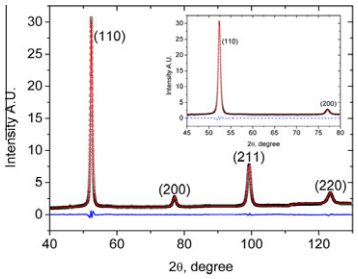


**Figure 3.** Typical measured (open circles) and fitted (thin red lines) XRD patterns of the as-drawn wire. The solid blue lines at the bottom of the figures are the difference between the measured and fitted data. The inset is the enlarged part with respect to the first two peaks, showing the fitting result.

Hence, positron trapping in α-ferrite dominates and the components resolved in PAS spectra correspond mainly to positrons annihilated in the α-ferrite phase.

Lifetimes ($\tau_i$) and relative intensities ($I_i$) of the components resolved in PAS spectra are listed in Table 1. The short-lived component with lifetime $\tau_1$ detected in the as-patented wire represents a contribution of free positrons annihilating in a delocalized state, i.e. not trapped at defects. The longer lifetime component with lifetime $\tau_2$ is the dominating contribution in both the as-patented and the as-drawn wire. The lifetime $\tau_2 \approx 157$ ps of this component is on the one hand very similar to the reported lifetimes of positrons trapped at dislocations in deformed iron, e.g. 165 ps [29] and $(150 \pm 4)$ ps [30], but on the other hand it is also quite close to the lifetime of positrons trapped at vacancy–carbon complexes observed in electron-irradiated iron containing carbon, i.e. 160 ps [29]. To clarify the nature of defects contributing to this component, the wires were annealed at 573 K, which is the dissociation temperature of vacancy–carbon complexes in carbon-doped iron [29,31,32]. Further PAS examinations of the annealed wires indicated that the annealing treatment did not lead to a significant change in $I_2$ (see Table 1), suggesting that the component with the lifetime $\tau_2$ corresponds to positrons trapped at dislocations. The as-drawn wire exhibits saturated positron trapping. Besides $\tau_2$, a long-lived component with lifetime $\tau_3 = 280$ ps was detected in the as-drawn wire, which corresponds to the contribution of positrons trapped at vacancy clusters. Comparison with theoretical calculations [33,34] revealed that lifetime $\tau_3$ corresponds to vacancy clusters consisting

**Table 1.** Measured $\tau_i$ and $I_i$ of the components resolved in the wires.

| Samples | $\tau_1$ (ps) | $I_1$ (%) | $\tau_2$ (ps) | $I_2$ (%) | $\tau_3$ (ps) | $I_3$ (%) |
|---|---|---|---|---|---|---|
| As-patented wire | $69 \pm 6$ | $21 \pm 2$ | $157 \pm 2$ | $79 \pm 1$ | – | – |
| As-patented wire annealed at 573 K | $58 \pm 6$ | $16 \pm 1$ | $159 \pm 3$ | $84 \pm 1$ | – | – |
| As-drawn wire | – | – | $156.5 \pm 0.9$ | $92 \pm 1$ | $280 \pm 10$ | $8 \pm 1$ |
| As-drawn wire annealed at 573 K | $55 \pm 9$ | $10.7 \pm 0.7$ | $150 \pm 0.7$ | $89.3 \pm 0.6$ | – | – |

of about nine vacancies. The disappearance of the long-lived component after the annealing treatment at 573 K (Table 1) implies that these vacancy clusters dissociated and the generated vacancies disappeared in sinks. Below, the concentration of the vacancies in the clusters in the as-drawn wire will be estimated.

There is a competition between the positrons trapped at dislocations and vacancy clusters. Because of the saturated positron trapping, the ratio of positron trapping rates in these two types of defects is equal to the ratio of intensities of the corresponding components in the positron lifetime spectrum [11],

$$\frac{K_{VC}}{K_D} = \frac{I_3}{I_2} \tag{1}$$

where $K_{VC}$ and $K_D$ are the positron trapping rates for vacancy clusters and dislocations, respectively. Positron trapping rates are directly related to defect densities:

$$K_{VC} = v_{VC} C_{VC} \tag{2}$$

$$K_D = v_D \rho_D \tag{3}$$

where $C_{VC}$ is the concentration of vacancy clusters and $\rho_D$ is the mean dislocation density. The symbols $v_{VC}$ and $v_D$ stand for the specific trapping rates (positron trapping coefficient) for the vacancy clusters and dislocations, respectively. Eqs. (1)–(3) yield

$$C_{VC} = \frac{v_D}{v_{VC}} \frac{I_3}{I_2} \rho_D \tag{4}$$

Hence, the concentration of vacancy clusters can be calculated from Eq. (4) if $v_{VC}$ and $v_D$ are known. First we estimate the specific trapping rate $v_D$. Since saturated positron trapping does not occur in the as-patented wire, $v_D$ in the as-patented wire can be calculated from PAS data using the two-state simple trapping model [11].

$$v_D = \frac{1}{\rho_D} \times \frac{\tau_{mean} - \tau_B}{\tau_2 - \tau_{mean}} \times \frac{1}{\tau_B} \tag{5}$$

where $\tau_B = 110$ ps [29] is the free positron lifetime in a well-annealed iron and $\tau_{mean} = \tau_1 I_1 + \tau_2 I_2$ is the mean positron lifetime in the as-patented wire. Using dislocation density $\rho_D = (8 \pm 2) \times 10^{14}\ m^{-2}$, determined in the as-patented wire by XLPA, one obtains from Eq. (5) the specific positron trapping rate for dislocations $v_D = (2.0 \pm 1.0) \times 10^{-5}\ m^2\ s^{-1}$. This value is comparable to that determined in low alloy Cr–Mo–V ferritic steels, $v_D = 3.6 \times 10^{-5} m^2\ s^{-1}$ [35], but is lower than that in high-purity iron ($5.1 \times 10^{-5}$–$7 \times 10^{-5}\ m^2\ s^{-1}$) [36]. This may be caused by the formation of Cottrell atmospheres [37], which reduces the probability of positron trapping at dislocations and is reflected in the lowered $v_D$.

The specific positron trapping rate for a small vacancy cluster consisting of $N$ vacancies ($N \leqslant 10$) increases linearly with the number of vacancies [38], i.e. $v_{CV} = N\, v_V$, where $v_V$ is the specific trapping rate for monovacancy. Vehanen et al. [29] compared their PAS data on electron-irradiated iron with electrical resistivity experiments [39] and derived the specific trapping rate for Fe vacancy of $(1.1 \pm 0.2) \times 10^{15}\ s^{-1}$. This value is relatively high and protrudes from the specific trapping rates ($v_C$) reported for many other metals, e.g. $1 \times 10^{14}\ s^{-1}$ for Cu [40], $2 \times 10^{14}\ s^{-1}$ for Ag [41], $2 \times 10^{14}\ s^{-1}$ for Au [42,43] and $(2–3) \times 10^{14}\ s^{-1}$ for Al [42,44,45]. In most metals $v_C$ is of the order of $10^{14}\ s^{-1}$. The value for iron derived by Vehanen et al. [29], which is almost 10 times higher than that of most metals, is to the authors' knowledge the highest value reported for vacancy in metals and may be overestimated. Hence, in this paper we conservatively assume that $v_V$ for Fe vacancy falls somewhere in the interval of $10^{15}$–$10^{14}\ s^{-1}$.

Using Eq. (4), one obtains the concentration of vacancy clusters in the as-drawn wire, which falls in the range of $10^{-6}$–$10^{-5}$. Since each cluster consists of approximately $N \approx 9$ vacancies, the concentration of vacancies which formed vacancy clusters in the as-drawn wire is $C_V = N\, C_{VC}$ and falls in the interval of $10^{-5}$–$10^{-4}$. This value is many orders of magnitude higher than the equilibrium concentration of thermal vacancy, which is less than $10^{-20}$ for Fe–C at room temperature [46]. We emphasize that the vacancy concentration estimated in this study represents only those vacancies created during plastic deformation, which subsequently agglomerate with other vacancies into clusters.

Saada estimated the concentration of point defects ($c_P$) created by plastic deformation as [47]:

$$c_P \approx \frac{A}{G} \int_0^{\varepsilon_{max}} \sigma d\varepsilon \tag{6}$$

where $A$ is the prefactor, $\sigma$ and $\varepsilon$ is the external stress and the strain applied, $G \approx 80$ GPa is the shear modulus of high carbon steel and $\int \sigma d\varepsilon \approx \frac{1}{2} \sigma_{max} \varepsilon_{max}$ with $\sigma_{max}$ the maximum stress and $\varepsilon_{max}$ the maximum strain. Since Eq. (6) is an integration of the incremental strain $d\varepsilon$, $\varepsilon_{max}$ equals to the value of true strain, i.e. $\varepsilon = 3$. As the true stress of α-ferrite in pearlitic steel wire is not available, $\sigma_{max} = 0.78$ GPa, which corresponds to the true stress of bcc iron-carbon steel at $\varepsilon = 3$ [48], was used for the estimation of Eq. (6) the prefactor $A$ was chosen as $10^{-2}$ at room temperature [49]. Then Eq. (6) leads to a value of $c_P$ in the order of $10^{-4}$. Since this latter approximated expression is a lower limit for the true integral, we can take the number given in Eq. (6) as the number of point defects that is most probably reached. This value is higher than the value measured by PAS. One possible explanation for this deviation could be an inherent problem of PAS in not detecting isolated vacancy–carbon pairs in the Fe–C system. First principles calculations [50] show that two C-atoms at one vacancy

form a C–C bond within the vacancy and therefore increase the electron density within the vacancy with a concomitant decrease in the positron life time. This is in agreement with experimental observations, where vacancies having more than one C-atom attached could not be detected by PAS [29].

In summary, combining XRD and PAS methods, the vacancy concentration of α-ferrite of a cold-drawn pearlitic steel wire with $\varepsilon = 3$ was determined to be $10^{-5}$–$10^{-4}$. These deformation-induced vacancies were identified quantitatively as being agglomerated to vacancy clusters in α-ferrite of cold-drawn pearlitic steel wire.

The authors are grateful for financial support by the Deutsche Forschungsgemeinschaft with SFB 602, project B13, the Ministry of Schools, Youths and Sports of the Czech Republic (project No. 0021620834) and The Academy of Science of the Czech Republic (projects No. KAN300100801). Financial support by the Alexander von Humboldt Stiftung is gratefully acknowledged by Y.Z.C. and S.G. We would also like to thank Dr. S. Nishida, Dr. H. Tashiro and Dr. K. Nakamura from Nippon Steel Corporation for providing the steel wire specimens. The authors appreciate the discussions with and continuing interest of Prof. Dierk Raabe, Dr. Yujiao Li and Dr. Pyuck Choi.

[1] C. Borchers, T. Al-Kassab, S. Goto, R. Kirchheim, Mater. Sci. Engr. A 502 (2009) 131.
[2] T. Tarui, N. Maruyama, J. Takahashi, S. Nishida, H. Tashiro, Nippon Steel Tech. Rep. 91 (2005) 56.
[3] M.H. Hong Jr, W.T. Reynolds, T. Tarui, K. Hono, Metall. Mater. Trans. A 30 (1999) 717.
[4] H.G. Read Jr, W.T. Reynolds, K. Hono, T. Tarui. Scripta Mater. 37 (1997) 1121.
[5] V.T.L. Buono, M.S. Andrade, B.M. Gonzalez, Metall. Mater. Trans A 29A (1998) 1415.
[6] V.G. Gavriljuk, V.G. Prokopenko, O.N. Rayumov, Phys. Stat. Sol. (a) 53 (1979) 147.
[7] V.G. Gavriljuk, Scripta Mater. 45 (2001) 1469.
[8] C. Borchers, Y. Chen, M. Deutges, S. Goto, R. Kirchheim, Phil. Mag. Lett. 90 (2010) 581.
[9] M. Nagumo, K. Ohta, H. Saitoh, Scripta Mater. 40 (1999) 313.
[10] P. Haasen, Phy. Metall., Cambridge University Press, Cambridge, 1996.
[11] R.N. West, in: P. Hautojärvi (Ed.), Positrons in Solids, Springer-Verlag, Berlin, 1979, p. 89.
[12] T. Ungár, G. Tichy, Phys. Phys. Stat. Sol. (a) 171 (1999) 425.
[13] L. Li, T. Ungár, Y.D. Wang, G.J. Fan, Y.L. Yang, N. Jia, Y. Ren, G. Tichy, J. Lendvai, H. Choo, P.K. Liaw, Scripta Mater. 60 (2009) 317.
[14] T. Ungár, J. Gubicza, G. Ribárik, A. Borbély, Appl. Crystallogr. 34 (2001) 298.
[15] E. Schafler, G. Steiner, E. Korznikova, M. Kerber, M.J. Zehetbauer, Mater. Sci. Eng. A 410–411 (2005) 169.
[16] S. Goto, R. Kirchheim, T. Al-Kassab, C. Borchers, Trans. Nonferrous Met. Soc. China 17 (2007) 1129.
[17] T. Ungár, M.G. Glavicic, L. Balogh, K. Nyilas, A.A. Salem, G. Ribárik, S.L. Semiatin, Mater. Sci. Engr. A 493 (2008) 79.
[18] F. Becvar, J. Cizek, I. Prochazka, Appl. Surf. Sci. 255 (2008) 111.
[19] I. Prochazka, I. Novotny, F. Becvar, Mater. Sci. Forum 772 (1997) 255.
[20] K. Williamson, W.H. Hall, Acta Metall. 22 (1953) 1.
[21] M. Wilkens, H.Z. Eckert, Naturforsch 19a (1964) 459.
[22] L. Balogh, G. Ribárik, T. Ungár, J. Appl. Phys. 100 (2006) 023512.
[23] G. Ribárik, J. Gubicza, T. Ungár, Mater. Sci. Eng. A387–A389 (2004) 343.
[24] http://www.renyi.hu/cmwp/
[25] T. Ungár, I. Dragomir, A. Révész, A. Borbély, J. Appl. Crystallogr. 32 (1999) 992.
[26] M.J. Puska, M. Sob, G. Brauer, T. Korhonen, Phys. Rev. B 49 (1994) 10947.
[27] B. Bergensen, E. Pajane, P. Kubica, M.J. Stott, C.H. Hodges, Solid State Commun. 15 (1974) 1377.
[28] R. Krause-Rehberg, V. Bondarenko, E. Thiele, R. Klemm, N. Schell, Nucl. Instrum. Methods Phys. Res. B 240 (2005) 719–725.
[29] A. Vehanen, P. Hautojärvi, J. Johansson, J. Yli-Kauppila, P. Moser, Phys. Rev., B 25 (2) (1982) 762.
[30] C. Hidalgo, G. Gonzalez-Doncel, S. Linderoth, J. San Juan, Phys. Rev. B 45 (1992) 7017.
[31] S. Takaki, J. Fuss, H. Kugler, H. Dedek, H. Schultz, Rad. Eff. 79 (1983) 87.
[32] T. Takeyama, H. Takahashi, in: M.T. Robinson, F.W. YoungJr. (Eds.), Fundamental Aspects of Radiation Damage in Metals, Energy Research and Development Administration, Oak Ridge, TN, 1976, p. 1100, CONF-751006.
[33] M.J. Puska, R.M. Nieminen, J. Phys. F: Met. Phys. 13 (1983) 333.
[34] A. Hempel, M. Hasegawa, G. Brauer, F. Plazaola, M. Saneyasu, Z. Tang, in: S. Bruemmer, P. Ford, G. Was (Eds.), Proceedings of the Ninth International Conference on "Environmental Degradation of Materials in Nuclear Power Systems – Water Reactors", August 1–5, 1999, Newport Beach, CA, The Minerals, Metals and Materials Society, 184 Thorn Hill Road Warrendale, Pennsylvania, 1999.
[35] J. Cizek, I. Procházka, J. Koccaroník, E. Keilová, Phys. Stat. Sol. (a) 651 (2000) 178.
[36] Y.-K. Park, J.T. Waber, M. Meshii, C.L. Snead Jr., C.G. Park, Phys. Rev. B34 (1986) 823.
[37] A.H. Cottrell, B.A. Bilby, Proc. Phys. Phys. Soc. A 62 (1949) 49.
[38] R.M. Nieminen, J. Laakonen, Appl. Phys. 20 (1979) 181.
[39] M. Weller, J. Diehl, P. Moser, M. Dubus, P. Hivert, in: C.C. Smith (Ed.), Internal Friction and Ultrasonic Attenuation in Solids, Pergamon, New York, 1980, p. 181.
[40] J.-E. Kluin, T. Hehenkamp, Phys. Rev. B 44 (1991) 11597.
[41] J. Wolff et al., Mater. Sci. Forum 105–110 (1992) 1329.
[42] T.M. Hall, A.N. Goland, C.L. Snead Jr., Phys. Rev. B 10 (1974) 3062.
[43] T.M. Hall, A.N. Goland, K.C. Jain, R.W. Siegel, Phys. Rev. B 12 (1975) 1613.
[44] E. Gramsch, K.G. Lynn, Phys. Rev. B 40 (1989) 2537.
[45] J.A. Jackman, G.M. Hood, R.J. Schultz, J. Phys. F 17 (1987) 1817.
[46] C.J. Först, J. Slycke, K.J. vav Vliet, S. Yip, Phys. Rev. Lett. 96 (2006) 175501.
[47] G. Saada, Acta Metall. 9 (1965) 166;
G. Saada, Acta Metall. 9 (1965) 965.
[48] G. Langford, M. Cohen, Trans. ASM 62 (1969) 623.
[49] M. Zehetbauer, Key Eng. Mater. 97–98 (1994) 287.
[50] C. Domain, C.S. Becquart, J. Foct, Phy. Rev. B 69 (2004) 144112.